REPRESENTING THE SPECIFICATION OF INDUSTRIAL X-RAY COMPUTED TOMOGRAPHY WITH AMPLITUDE–WAVELENGTH SPACE

Herminso Villarraga-Gómez[1, 3], Lars Körner[2], Richard Leach[2], and Stuart T. Smith[1]
[1]Center for Precision Metrology, University of North Carolina at Charlotte, NC, USA
[2]Manufacturing Metrology Team, University of Nottingham, Nottingham, UK
[3]Nikon Metrology, Inc., Brighton, MI, USA

INTRODUCTION

With its main advantage being the ability to perform nondestructive measurement of parts' internal features, X-ray computed tomography (CT) is becoming established in the field of dimensional metrology [1-5]. The current approach being applied by ISO working group 213, to allow comparison of CT with other traditional measuring systems, such as tactile coordinate measuring machines (CMMs) or optical measuring instruments, is that its metrological performance should be quantified using verification tests that resemble some common features of the current standardized techniques, such as those in ISO 10360 part 2 [6-7]. The VDI/VDE 2630-1.2 guidelines [10] are an example of an approach that is designed to extend the ISO 10360 series to the field of X-ray CT metrology. But trying to implement CT verification tests as an extension of the ISO 10360-2 series, which were originally developed for tactile CMMs, presents several challenges, particularly because the physical principles of CT operation differ substantially from those of CMMs. Depending on the different types of interaction between the measuring sensor and the surfaces of the workpiece being measured, each technique has its own distinctive attributes that impact their capabilities and range of applications.

It is also necessary to compare the performance of instruments that have similar measuring capabilities but different operating principles. This has been achieved for CT systems by performing inter-laboratory comparisons [11-13], and additionally by testing a variety of calibrated workpiece artifacts and performing comparisons against CMM measurements, e.g., see [2, 8, 14-21]. It would be useful to have a single method that compares X-ray CT against the performance of other measurement technologies. Having such a method would also ease the choice of which instrument type to use in given situations. Fortunately there is a method to create such a comparison devised in the 1970s. The performance limits associated with each technique, in terms of their ability to measure surfaces, can be illustrated by using an amplitude-wavelength (AW) map or 'Stedman diagram' [22-26], a technique that creates a polygonal area enclosing the working capabilities of a measurement instrument for surfaces modeled as ideal sinusoids of varying amplitude A and wavelength W. Following the framework developed by Stedman, this paper proposes to map X-ray CT instrument performance to AW space. The general process is illustrated in Figure 4. To build the AW space, four key parameters are needed, which describe the maximum component size and the achievable resolution in all axes of operation. Due to the historic link to surface metrology, the range and resolution are evaluated in two directions. The naming for those two directions are amplitude and wavelength, i.e., A and W. Based on the naming convention of Stedman, those two directions have further associated names: horizontal for the wavelength direction and vertical for the amplitude. While this separation is often needed for other surface and dimensional metrology systems, in X-ray CT this separation of the principal directions can essentially be ignored. This assumption relies on the feature sizes being representative of a cubic volume that is isotropic in all aspects. Thus, for derivation of the AW space, the value for the parameters describing the horizontal and vertical directions are equal.

RANGE LIMITS, R_v AND R_h

The range limits of the maximum component size (R_v and R_h for the vertical and horizontal directions respectively) are set by estimating the maximum measuring range that can be covered by industrial X-ray CT instruments operating at source voltages ranging from 20 kV up to 450 kV, which is typically the range covered by current microfocus CT technologies. Although the energy spectra emitted by X-ray tube sources are inherently polychromatic, the penetration depth of the X-ray beam into a material can be estimated in terms of its effective energy E_{eff} [27]. Assuming a narrow and quasi-monochromatic beam of energy E_{eff} passing through a slab of homogeneous material of density ρ, the attenuation of intensity in the X-ray beam can be described by the Beer-Lambert law:

$$I(x) = I_0 \cdot e^{-\mu \cdot x}, \qquad (1)$$

where I_0 denotes the intensity of the incident X-ray beam, $I(x)$ the intensity of the beam after passing through a length x within the slab, and μ the linear attenuation coefficient of the slab's material. The linear attenuation coefficient is expressed in inverse length units (cm^{-1}), but instead of μ, the mass attenuation coefficient $\mu_m = \mu/\rho$, with ρ the density of the absorber material, is more commonly found in current databases. The mass attenuation coefficient is energy and material dependent, i.e., $\mu_m = \mu_m(E, Z_{eff})$, where E represents the energy of the incident radiation and Z_{eff} the effective atomic number of the material. Therefore, for a given material of density ρ, the attenuation coefficient $\mu = \rho \cdot \mu_m(E, Z_{eff})$ is also dependent on the X-ray beam energy that passes through it and the material composition.

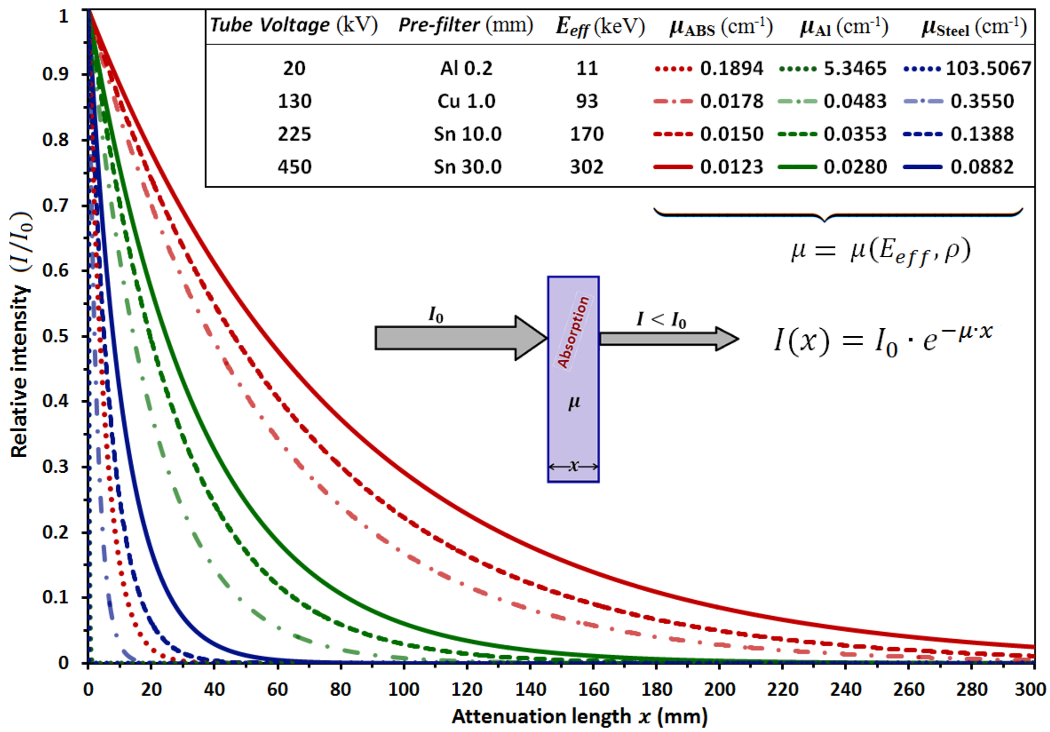

FIGURE 1. Attenuation curves for X-ray beams of different energies (as listed in the inset box), under the assumption of monochromaticity, when they pass through a length x in homogeneous materials of different types: ABS (acrylonitrile butadiene styrene), aluminum (Al), and steel 316L.

Figure 1 shows the attenuation curves associated with X-ray beams of different energies E_{eff} passing through a length x in homogeneous materials of different types. For simplicity, in lieu of using a polychromatic simulation, a monochromatic computation is presented here. The full spectrum of the incident photons from the tungsten X-ray tube is simplified to a beam of photons all having the same energy. The effective energies E_{eff} used for the computations of the attenuation curves are shown in Figure 1, and were calculated by using a recently developed simulation tool that, based on interpolating cubic spline polynomials, computes the spectra generated by tungsten target X-ray tubes [27]. The input quantities required to run the simulation are tube voltage, pre-filtration thickness, and the type of filter material. The third column of the inset table of Figure 1 shows four effective energy results E_{eff} that correspond to tube voltages of 20 kV, 130 kV, 225 kV, and 450 kV, with different combinations of hardware pre-filtration. Using these energy values E_{eff}, the attenuation coefficients μ of acrylonitrile butadiene styrene

(ABS), aluminum (Al), and steel were computed using data for the mass attenuation coefficient μ_m from the NIST database XCOM [28]. With these attenuation coefficients μ, the curves shown in Figure 1 were computed by using Eq. (1). Based on these results, the limits R_v and R_h fall into the 300 mm range for polymer materials. But as can also be seen in Figure 1, this range is smaller for workpieces made of metals, such as aluminum, and would be much smaller for heavy metals, such as steel alloys, nickel compounds, and cast iron materials. Thus, depending on the material composition and the maximum material thickness of the part, the maximum component size can be significantly smaller. An important feature of this assumption is that the penetration depth of X-rays is the limiting dimension of the CT technique, whereas the bounding dimensions of the component are often limited by the detector size. Therefore, it is also worth noting that the limits of R_v and R_h may be further restricted by the physical size of X-ray detectors, which in cone-beam acquisition setups—considered as an efficient configuration for volumetric CT—correspond to a flat planar detector.

RESOLUTION LIMITS, r_v AND r_h

The notion of the different resolutions is a heavily debated topic in X-ray CT, e.g., see [7, 29-38]. Thus, the selection of the figure of merit for the resolution limits (r_v and r_h for the vertical and horizontal directions respectively) is critical. Part of the ongoing debate on resolution, is the differentiation between measurable (metrological) 'structural resolution' and 'spatial resolution'. The spatial resolution, also named high-contrast resolution, is concerned with the resolving power on the grey-scale image/volume. It is defined by the modulation transfer function (MTF), which is a measure of how a system attenuates the amplitude of different spatial frequencies of the captured object during the imaging process. The left side of Figure 2 pictorially models the point spread function (PSF) response for a single pixel during the CT imaging process. The absolute value of the Fourier transform of the PSF gives the MTF, which is a direct and quantitative measure of the CT system's ability to transfer contrast at a particular spatial resolution through the imaging chain from the object to the image. There are a variety of CT configurations that can be used to achieve different spatial resolutions—in ranges from millimeters to nanometers (i.e., sub-micron level)—and fit different applications, e.g., see [4, 39]. In general, although the spatial resolution of CT scanning is limited by the size of the focal spot emanating the X-rays, nanometer resolutions can be achieved in the lower energy range with synchrotron X-ray sources or with the help of focusing elements, such as Fresnel zone plates or Kirkpatrick-Baez mirrors (e.g., see [39-42]).

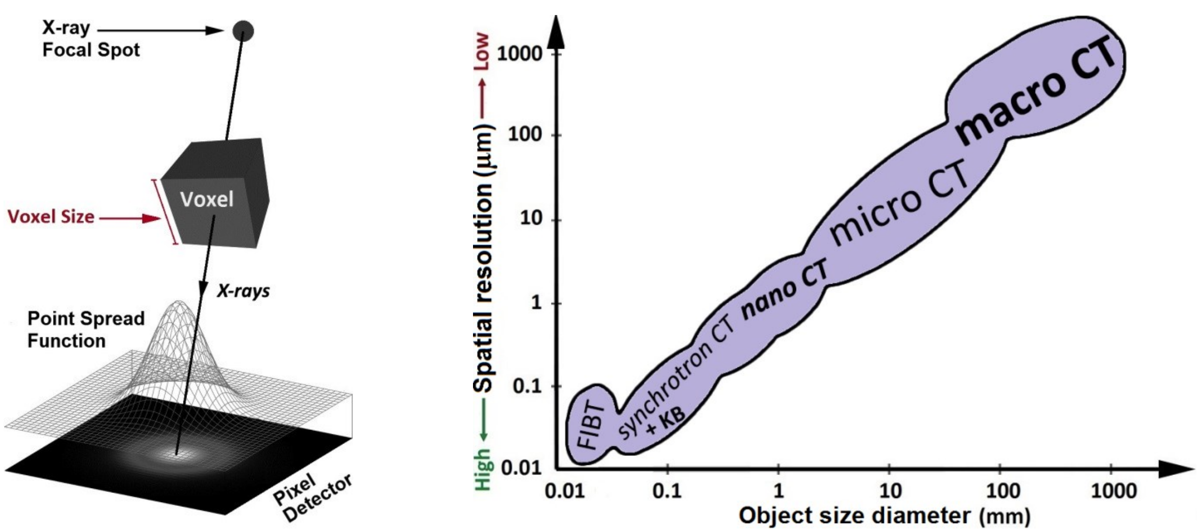

FIGURE 2. Left: Schematic representation of the point spread function (PSF) response for a voxel/pixel detection during CT aqcuisition. The Fourier transform of the PSF gives the MTF. Right: Typical spatial resolutions that are achievable by multi-scale CT as a function of sample size (based on [1, 4, 42]): conventional CT or macro CT (>10 µm), micro CT (currently >3 µm), nano CT (currently >0.4 µm), synchrotron CT (currently >0.2 µm), synchrotron CT with Kirkpatrick–Baez mirrors (currently >0.04 µm), and focused ion beam tomography (FIBT, currently >0.01 µm).

The right side of Figure 2, for example, depicts the typical spatial resolutions (as a function of sample size) achievable by current technologies of multi-scale CT. However, this high-contrast resolution does not capture the entirety of a measurement process for metrology tasks that involve high dimensional accuracy. In the current state of the art of dimensional metrology, the uncertainties associated with measurements of length are typically in the range of a few to several tenths of micrometers [1, 11-13]. It is actually the concept of 'structural resolution' that defines the size of the smallest structures that can be measured dimensionally. The concept of structural resolution necessarily includes the entire measurement chain—including the surface determination stage [1]. Approaches to measure the structural resolution of X-ray CT metrology systems have been proposed by several institutions. All proposed methods require a dedicated artifact. Some artifacts aiming to create a surface texture of known spatial frequency spectrum have been investigated elsewhere [32, 34-37, 43]. While these methods can help with understanding how spatial frequencies will be transmitted through the measurement chain, different figures of merit can be obtained from those transfer characteristics. Other artifacts are based on obtaining a value for the smallest radius/diameter that can be measured. Here, concepts include the use of sharp edges, and evaluate how the measurement chain will approximate it as a radius, or to study the smallest sphere for which a diameter can be computed. The two-spheres (or 'Hourglass') method is another way to determine structural resolution [7, 31], see Figure 3. In this method, the interface of two spheres is measured using CT. If the interface is measured using a measurement system of infinite resolution, the contact area measured should be equal to the Hertzian contact area. However, the measurement chain will degrade this interface, and the contact area can be approximated by knowing its diameter and height values. Given that the theoretical Hertzian contact area can be shown to be less than a nanometer [31], length of the interface diameter can be considered an appropriate estimation of the metrological structural resolution, i.e., the smallest measurable feature. Several values with different levels of error margin in each resolution assessment are reported elsewhere [31], showing that, by using a modern microfocus CT system with an acceleration voltage of 210 kV, the limiting structural resolution (the CT interface of two spheres)—at the highest magnification—can be considered to be around 10 μm.

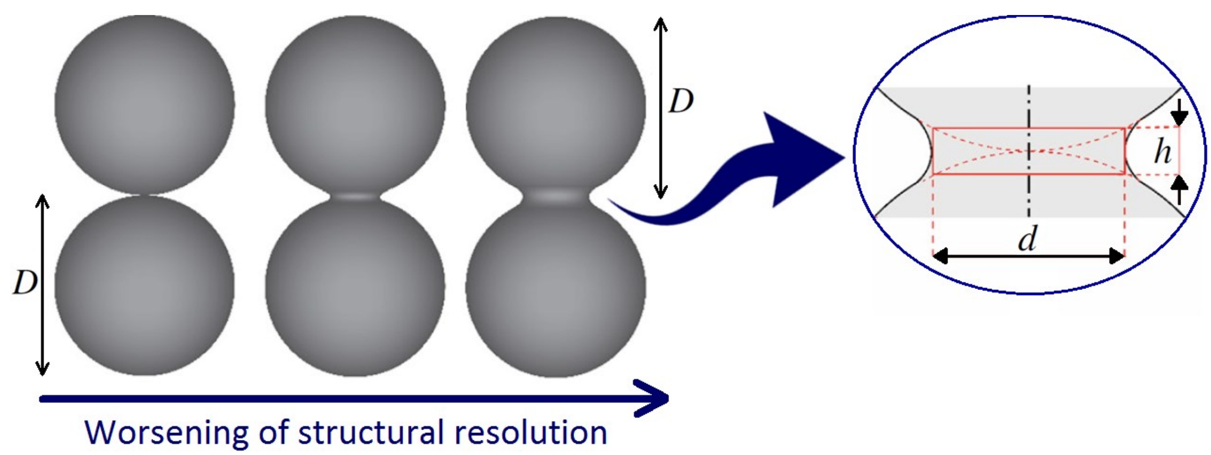

FIGURE 3. The two-spheres (or 'Hourglass') *method for evaluating the metrological structural resolution in dimensional CT [7, 31]. A worsening of the structural resolution will affect the measured interface of the two interfacing spheres with diameter D. The approximated interface region can be described by two parameters, the height of the interface region h and the apparent diameter of the interface d. Hence, when the resolution of the measurement system worsens, the measured interface diameter will increase.*

In the calculations in this work, the metrological structural resolution has been used as the resolution limits (r_{v} and r_{h})—as opposed to the high-contrast resolution, as the structural resolution represents the entire measurement chain. While the resolution is affected by many system and operator variables, this paper uses numerical values for r_{v} and r_{h} that approach the most ambitious values of structural resolution for X-ray CT dimensional metrology that are reported in recent literature [31], i.e., 10 μm. However, the authors of this paper are aware that these are *optimistic* values, which might not be achievable for all combinations of materials, component size, and resolution and system setups. With these considerations, this paper proposes to use the smallest and most optimistic interface radius of the hourglass approach ($R_{\min}$) as the resolution limit of X-ray CT in AW space to cover a large-range of metrology inspection applications that could be performed with X-ray CT. Since the smallest achievable interface diameter that can be measured in the hourglass artifact, according to recent literature [31], is of the order of 10 μm, the proposed value of $R_{\min}$ for the calculations of the AW space presented in this paper equates to 5 μm. The calculations following Stedman also require a largest radius measurable by the instrument. The authors assume that there are no limitations on the ability of measuring flat surfaces when using CT, except, perhaps, by the presence of cone-beam (or Feldkamp) artifacts, which generally can be minimized by tilting the measuring object with respect to the CT rotating axis [1]. Therefore, in the derivation of the AW space presented below, $R_{\max}$ was set to an arbitrary large value.

THE AMPLITUDE–WAVELENGTH MAP

Based on Fourier analysis, and for mathematical convenience, surface profiles can be modeled as a superposition of ideal sinusoids of the form,

$$y_n = A_n \cdot \sin(2\pi x/W_n), \tag{2}$$

where A_n and W_n are their amplitudes and wavelengths respectively. Surface slopes and curvatures can be derived by first and second order derivatives, respectively, i.e.,

$$S = \frac{dy_n}{dx} = \left(\frac{2\pi A_n}{W_n}\right) \cdot \cos(2\pi x/W_n), \tag{3}$$

$$C = \frac{d^2 y_n}{d^2 x} = -\left(\frac{4\pi^2 A_n}{W_n^2}\right) \cdot \sin(2\pi x/W_n). \tag{4}$$

In equations (3) and (4) the maximum slope $S_{\max}$ and minimum radius of curvature $R_{\min}$ occur at

$$S_{\max} = 2\pi A_n/W_n, \tag{5}$$

$$1/R_{\min} = 4\pi^2 A_n/W_n^2. \tag{6}$$

To cover a wide-range of values of A_n and W_n, the AW mapping [22-25] was originally designed to be a log-log plot. Therefore, by taking the logarithms of Eqs. (5) and (6), the straight lines of constant maximum slope $S_{\max}$ and constant minimum radius $R_{\min}$ that restrict the operating envelope of the AW space can be created. More specifically,

$$\log A_n = \log(S_{\max}/2\pi) + \log W_n, \tag{7}$$

$$\log A_n = \log(1/4\pi^2 R_{\min}) + 2 \cdot \log W_n, \tag{8}$$

are restricting boundaries of the AW polygonal area enclosing the working capabilities of a measurement instrument that is presumed to measure surfaces modeled by Eq. (2), and subject to the additional restrictions $R_{\mathrm{v}} > 2A_n > r_{\mathrm{v}}$ and $R_{\mathrm{h}} > W_n > 2r_{\mathrm{h}}$, see Figure 4. In Figure 4 (left), for the case of X-ray CT metrology instruments, $R_{\mathrm{v}} = R_{\mathrm{h}} \approx$ 300 mm and $r_{\mathrm{v}} = r_{\mathrm{h}} = R_{\min} \approx$ 5 μm, as explained in the preceding sections. The maximum slope limit $S_{\max}$ of the sinusoidal surface (that could be measured by X-ray CT) was set to ~90° (i.e., $S_{\max} \approx$ 1.5708 rad). Given the volumetric nature of the imaging process of X-rays, slope angle limitations are assumed to be negligible. Hence the slope angle of 90° used for the calculations of the AW map is justified. In addition, as discussed in the previous section, $R_{\max}$ was set to an arbitrary large value given that, in principle, there are no limitations for X-ray CT to measure flat surfaces of constant (or mean) zero curvature.

As a last remark, it is worth noting that the values of R_{v}, R_{h}, r_{v}, r_{h}, $R_{\min}$, and $S_{\max}$, hypothetically (or tentatively) identified in this paper for X-ray CT technologies, are the limits currently observed in metrological practice and reported in the literature (including the optimistic values that may apply to the metrological structural resolution). In general, these limits may be further restricted by other considerations, such as the focal spot size of the X-ray source, degree of beam collimation, projection geometry, sample size, the physical size of X-ray detector, and the details of the reconstruction algorithms used for a particular CT application. In particular, in the context of metrology applications, it is of crucial importance to account for the measurement uncertainties typically observed in the current literature [1, 11-13] when setting the aforementioned limiting values (R_{v}, R_{h}, r_{v}, r_{h}, $R_{\min}$, and $S_{\max}$). At the same time, these boundaries could be extended—and their limiting values be pushed up or down—by new developments in technology, as long as metrological performance can be demonstrated for dimensional measurement tasks, in a way that is more comprehensive than simple optical image visualization (e.g., high contrast resolutions are currently achievable by multi-scale CT imaging technologies, see Figure 2, but these ‘resolutions’ cannot currently be tied to a one-to-one relationship for structural resolutions of metrological performance). The limiting factors for the other measurement technologies, as featured in Figure 4, were selected from published references [44-50]. However, the polygonal limiting boundaries in the figure are drawn only for illustration and will likely evolve with more comprehensive models of limiting factors in CT metrology.

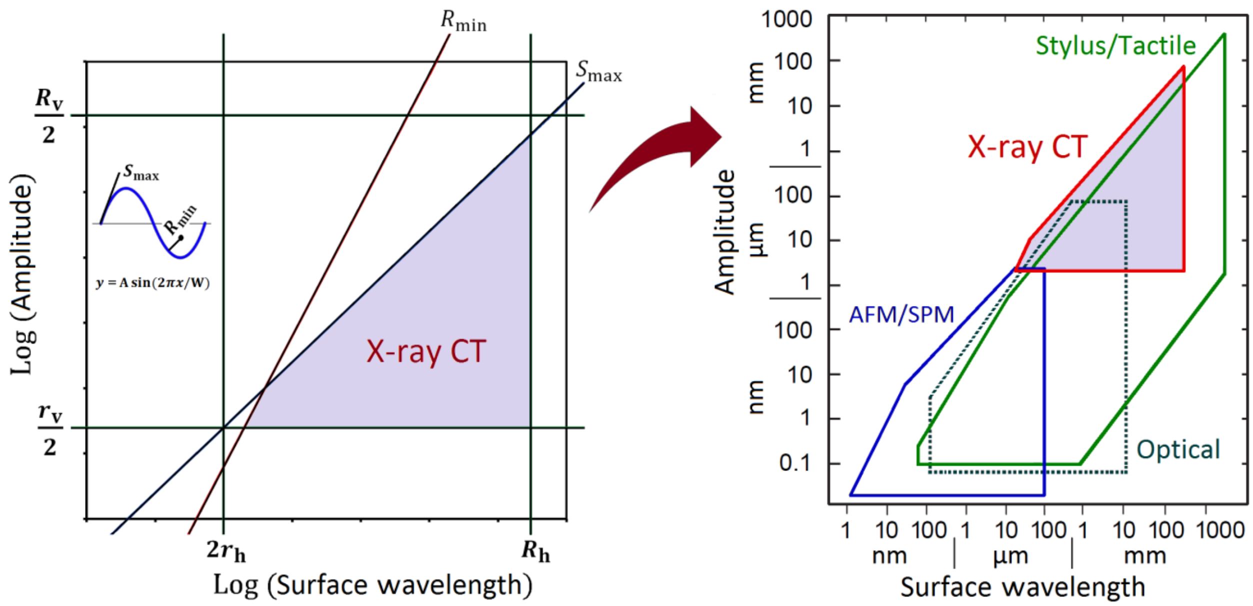

FIGURE 4. X-ray CT metrology performance represented in the Stedman (amplitude–wavelength) space. Left: Setting the parameter constraints. Right: Comparison of CT’s performance in amplitude–wavelength space with other dimensional metrology techniques that include mechanical stylus/tactile methods (from nanoscale stylus profilometry to large-scale CMMs), optical methods (optical profilometry, confocal microscopy, and interferometry), atomic force microscopy (AFM), and scanning probe microscopy (SPM).

CONCLUSIONS

This paper is an elaboration upon previously published work [1], which introduced a plot of industrial X-ray CT’s performance in amplitude-wavelength space for the first time (to the authors’ knowledge). This plot facilitates the comparison of X-ray CT competence with other traditional measuring techniques (e.g., tactile and optical methods), in terms of resolution and measuring range and, therefore, provides a quick overview of the limitations and capabilities of CT in the field of dimensional surface metrology. Such a comparison can be carried out without the study of often complex instrument specifications or lengthy performance comparisons. An AW plot (or AW map) provides only a generalized measure of performance for comparisons with other instruments. In a more comprehensive comparison, considerations of cost, measurement time (dynamics) [48], conformance with standards, and other unique characteristics that differentiate the different measuring processes should also be included. In particular, the CT technique is known to be susceptible to unwanted effects, namely CT artifacts, that emerge from discrepancies between the absorption values used for computing the CT data and the actual absorption (or attenuation) of the measuring object. CT artifacts can occur from influences like the component’s geometry and its orientation within the CT machine [1]. Such errors can be mapped in the Fourier domain and can affect metrological performance. These unwanted effects are not encapsulated in the AW map.

RKL and LK would like to acknowledge funding from the following grants of the EPSRC: EP/101534X/1 and EP/M008983/1.

REFERENCES

[1] H. Villarraga-Gómez, PhD Dissertation: Studies of Dimensional Metrology with X-ray CAT Scan, Department of Physics and Optical Science: The University of North Carolina at Charlotte, 2018.

[2] H. Villarraga-Gómez, C. Lee and S. T. Smith, "Dimensional metrology with X-ray CT: a comparison with CMM measurements on internal features and compliant structures," *Precision Engineering,* vol. 51, pp. 291-307, 2018.

[3] J. P. Kruth, M. Bartscher, S. Carmignato, R. Schmitt, L. De Chiffre and A. Weckenmann, "Computed tomography for dimensional metrology," *CIRP Annals - Manufacturing Technology,* vol. 60, no. 2, pp. 821-842, 2011.

[4] L. De Chiffre, S. Carmignato, J. P. Kruth, R. Schmitt and A. Weckenmann, "Industrial applications of computed tomography," *CIRP Annals - Manufacturing Technology,* vol. 63, no. 2, pp. 655-677, 2014.

[5] A. Buratti, J. Bredemann, M. Pavan, R. Schmitt and S. Carmignato, "Applications of CT for Dimensional Metrology," in *In Industrial X-Ray Computed Tomography (Eds: Carmignato S., Dewulf W., and Leach R.)*, Cham, Switzerland, Springer, 2018, pp. 333-369.

[6] M. Bartscher, M. Neukamm, U. Hilpert, U. Neuschaefer-Rube, F. Hartig, K. Kniel, K. Ehrig, A. Staude and J. Goebbels, "Achieving Traceability of Industrial Computed Tomography," *Key engineering Materials,* vol. 437, pp. 79-83, 2010.

[7] S. Carmignato, A. Pierobon, P. Rampazzo, M. Parisatto and E. Savio, "CT for Industrial Metrology - Accuracy and Structural Resolution of CT Dimensional Measurements," in *4th Conference on Industrial Computed Tomography (iCT)*, Wels, Austria, 2012.

[8] M. Bartscher, U. Hilpert, J. Goebbels and G. Weidemann, "Enhancement and proof of accuracy of industrial computed tomography (CT) measurements," *CIRP Annals - Manufacturing Technology,* vol. 56, no. 1, pp. 495-498, 2007.

[9] ISO 10360-2, Geometrical Product Specifications (GPS) - Acceptance and reverification tests for coordinate measuring machines (CMM) - Part 2: CMMs used for measuring linear dimensions, Geneva: ISO copyright office, 2009.

[10] VDI/VDE 2630-1.2, Computed Tomography on Dimensional Measurement - Influencing variables on measurement results and recommendations for computed-tomography dimensional measurements, Berlin: Beuth Verlag GmbH, 2010.

[11] S. Carmignato, A. Pierobon and E. Savio, "CT Audit: Interlaboratory Comparison of Computed Tomography Systems for Dimensional Metrology, Final Report," Laboratory of Industrial and Geometrical Metrology, University of Padova, Padova (Italy), 2012.

[12] J. Angel and L. De Chiffre, "Inter laboratory comparison on Industrial Computed Tomography: CIA-CT comparison - Final report," DTU Mechanical Engineering, Technical University of Denmark, Kongens Lyngby (Denmark), 2013.

[13] A. Stolfi and L. De Chiffre, "InteraqCT Comparison on Assemblies - Final Report," DTU Mechanical Engineering, Technical University of Denmark, Kongens Lyngby (Denmark), 2016.

[14] S. Carmignato, D. Dreossi, L. Mancini, F. Marinello, G. Tromba and E. Savio, "Testing of x-ray microtomography systems using a traceable geometrical standard," *Measurement Science and Technology,* vol. 20, no. 8, p. 084021 (7pp), 2009.

[15] K. Kiekens, F. Welkenhuyzen, Y. Tan, P. Bleys, A. Voet, J. Kruth and W. Dewulf, "A test object with parallel grooves for calibration and accuracy assessment of industrial computed tomography (CT) metrology," *Measurement Science and Technology,* vol. 22, no. 11, p. 115502 (7pp), 2011.

[16] M. Bartscher, M. Neukamm, M. Koch, U. Neuschaefer-Rube, A. Staude, J. Goebbels, K. Ehrig, C. Kuhn, A. Deffner and A. Knoch, "Performance assessment of geometry measurements with micro-CT using a dismountable work-piece-near reference standard," in *10th European Conference on Non-Destructive testing*, Moscow, Russia, 10pp, 2010.

[17] A. Voet, K. Kiekens, F. Welkenhuyzen, Y. Tan, W. Dewulf and J. P. Kruth, "A test object for calibration and accuracy assessment in X-ray CT metrology," in *10th International Symposium on Measurement and Quality Control*, Osaka (Japan), 4pp, 2010.

[18] A. Staude, J. Goebbels, K. Ehrig, M. Bartscher, M. Koch and U. Neuschaefer-Rube, "A new test piece for geometry and defect measurements with micro-CT," in *10th European Conference on Non-Destructive testing*, Moscow, Russia, 8pp, 2010.

[19] S. Carmignato, A. Pierobon, F. Marinello and E. Savio, "Olympic Gauge: A New Reference Standard for Testing X-ray Microtomography Systems," in *10th Euspen international conference*, Delft (Netherlands), pp. 217-220, 2010.

[20] F. Léonard, S. B. Brown, P. J. Withers, P. M. Mummery and M. B. McCarthy, "A new method of performance verification for x-ray computed tomography measurements," *Measurement Science and Technology,* vol. 25, no. 6, p. 065401 (10pp), 2014.

[21] P. Müller, J. Hiller, A. Cantatore, G. Tosello and L. De Chiffre, "New reference object for metrological performance testing of industrial CT systems," in *12th Euspen International Conference*, Stockholm (Sweden), 4pp, 2012.

[22] M. Stedman, "Basis for comparing the performance of surface-measuring machines," *Precision Engineering,* vol. 9, no. 3, pp. 149-152, 1987.

[23] M. Stedman, "Mapping the performance of surface-measuring instruments," in *Proc. SPIE Vol. 803, Proc. of Micromachining of Elements with Optical and Other Submicrometer Dimensional and Surface Specifications*, The Hague (Netherlands), pp. 138-142, 1987.

[24] A. Franks, "Nanometric surface metrology at the national physical laboratory," *Metrologia,* vol. 28, no. 6, pp. 471-482, 1991.

[25] S. Rosén, T. R. Thomas and B.-G. Thomas, "The Stedman diagram revisited," *Surface Topography: Metrology and Properties,* vol. 2, p. 014005 (5pp), 2013.

[26] A. Blum and C. Evans, "The history and future of the Stedman diagram," in *Proc. of ASPE - Spring Topical Meeting*, Tucson, Arizona (USA), pp. 26-31, 2017.

[27] A. M. Hernandez and J. M. Boone, "Tungsten anode spectral model using interpolating cubic splines: unfiltered x-ray spectra from 20 kV to 640 kV," *Medical Physics,* vol. 41, no. 4, p. 042101 (15p), 2014.

[28] M. J. Berger, J. H. Hubbell, S. M. Seltzer, J. Chang, J. S. Coursey, R. Sukumar, D. S. Zucker and K. Olsen, "XCOM: Photon Cross Section Database (version 1.5)," National Institute of Standards and Technology, Gaithersburg, MD, 2010. [Online]. Available: http://physics.nist.gov/xcom. [Accessed March 2018].

[29] M. Bartscher, H. Bremer, T. Birth, A. Staude and K. Ehrig, "The resolution of dimensional CT - An edge-based analysis," in *4th Conference on Industrial Computed Tomography* , Wels - Austria, 2012.

[30] VDI/VDE 2630-1.3, Computed Tomography in Dimensional Measurement - Guideline for the application of DIN EN ISO 10360 for coordinate measuring machines with CT sensors, Berlin (Germany): Beuth Verlag GmbH, 2011.

[31] F. Zanini and S. Carmignato, "Two-spheres method for evaluating the metrological structural resolution in dimensional computed tomography," *Measurement Science and Technology,* vol. 28, p. 114002 (9pp), 2017.

[32] F. A. Arenhart, V. C. Nardelli, G. D. Donatelli, M. C. Porath, C. Isenberg and R. Schmitt, "Design of a Multi-Wave Standard for Evaluating the Frequency Response of CT Measuring Systems," in *11th ISMQC*, Cracow-Kielce, Poland, 2013.

[33] J. Illemann, M. Bartscher, O. Jusko, F. Härtig, U. Neuschaefer-Rube and K. Wendt, "Procedure and reference standard to determine the structural resolution in coordinate metrology," *Meas. Sci. Technol.,* vol. 25, no. 6, 2014.

[34] M. Flessner, N. Vujaklija, E. Helmecke and T. Hausotte, "Determination of metrological structural resolution of a CT system using the frequency response on surface structures," in *MacroScale*, Vienna, Austria, 2014.

[35] F. A. Arenhart, V. C. Nardelli and G. D. Donatelli, " Characterization of the surface content transfer function of CT measuring systems," in *Conference on Industrial Computed Tomography*, Wels, Austria, 2014.

[36] F. A. Arenhart, V. C. Nardelli and G. D. Donatelli, "Characterization of the metrological structural resolution of CT systems using a multi-wave standard," in *XXI IMEKO World Congress "Measurement in Research and Industry"*, Prague, Czech Republic, 2015.

[37] F. A. Arenhart, C. R. Baldo, T. L. Fernandes and G. D. Donatelli, "Experimental Investigation of the Influencing Factors on the Structural Resolution for Dimensional Measurements with CT Systems," in *6th Conference on Industrial Computed Tomography*, Wels - Austria, 2016.

[38] M. Bartscher, O. Sato and F. U. Härtig, "Current state of standardization in the field of

dimensional computed tomography," *Measurement Science and Technology,* vol. 25, no. 6, p. 064013 (14pp), 2014.

[39] E. Maire and P. J. Withers, "Quantitative X-ray tomography," *International Materials Reviews,* vol. 59, no. 1, pp. 1-43, 2014.

[40] P. J. Withers, "X-ray nanotomography," *Materials Today,* vol. 10, no. 12, pp. 26-34, 2007.

[41] G. E. Ice, J. D. Budai and J. W. L. Pang, "The race to X-ray microbeam and nanobeam science," *Science,* vol. 334, no. 6060, pp. 1234-1239, 2011.

[42] J. Kastner and C. Heinzl, "X-ray Computed Tomography for Non-destructive Testing and Materials Characterization," in *Integrated Imaging and Vision Techniques for Industrial Inspection (Liu Z., Ukida H., Ramuhalli P., Niel K., editors)*, London, England (UK), Springer, 2015, pp. 227-250.

[43] F. A. Arenhart, V. C. Nardelli and G. D. Donatelli, "Comparison of surface-based and image-based quality metrics for the analysis of dimensional computed tomography data," *Case Studies in Nondestructive Testing and Evaluation,* vol. 6, pp. 111-121, 2016.

[44] S. Stedman and K. Lindsey, "Limits of surface measurement by stylus instruments," in *Proc. SPIE Vol. 1009, Surface Measurement and Characterization*, Hambur (Germany), pp. 56-61, 1988.

[45] M. Stedman, "Limits of topographic measurement by the scanning tunnelling and atomic force microscopes," *Journal of Microscopy,* vol. 152, no. 3, pp. 611-617, 1988.

[46] J. E. Griffith and D. A. Grigg, "Dimensional metrology with scanning probe microscopes," *Journal of Applied Physics,* vol. 74, no. 9, pp. R83-R109, 1993.

[47] T. R. Thomas, "Trends in surface roughness," *International Journal of Machine Tools and Manufacture,* vol. 38, no. 5-6, pp. 405-411, 1998.

[48] C. W. Jones and R. K. Leach, "Adding a dynamic aspect to amplitude–wavelength space," *Measurement Science and Technology,* vol. 9, no. 5, p. 055105 (7pp), 2008.

[49] S. H. R. Ali, "Advanced Nanomeasuring Techniques for Surface Characterization," *International Scholarly Research Notices (ISRN) Optics,* p. 859353 (pp23), 2012.

[50] R. K. Leach, C. L. Giusca, H. Haitjema, C. Evans and X. Jiang, "Calibration and verification of areal surface texture measuring instruments," *CIRP Annals,* vol. 64, no. 2, pp. 797-813, 2015.